

Optical properties of one- and two-dimensional photonic crystals based on silicon

F. MARABELLI⁽¹⁾, M. AGIO⁽¹⁾, L.C. ANDREANI⁽¹⁾, D. BAJONI⁽¹⁾, M. BELOTTI⁽¹⁾, M. GALLI⁽¹⁾, G. GUIZZETTI⁽¹⁾, M. PATRINI⁽¹⁾, L. PAVESI⁽²⁾, P. BETTOTTI⁽²⁾, L. DAL NEGRO⁽²⁾, Z. GABURRO⁽²⁾, G. PUCKER⁽³⁾, A. LUI⁽³⁾, P. BELLUTTI⁽³⁾, D. PEYRADE⁽⁴⁾, Y. CHEN⁽⁴⁾

⁽¹⁾ *INFM and Dipartimento di Fisica "A. Volta", Università di Pavia, 27100 Pavia, Italy*

⁽²⁾ *INFM and Dipartimento di Fisica, Università di Trento, 38050 Povo-Trento, Italy*

⁽³⁾ *ITC-IRST, 38050 Povo-Trento, Italy*

⁽⁴⁾ *Laboratoire de Photonique et de Nanostructures, LPN-CNRS, 91460 Marcoussis, France*

Summary. — A comparative investigation, both experimental and theoretical, of the optical properties of one- and two-dimensional photonic crystals based on silicon is presented. The samples consisted of: a) $(\text{Si}/\text{SiO}_2)_m$ multilayers with $m \leq 8$, in the $\lambda/4$ distributed Bragg configuration, grown on SiO_2 wafers by low-pressure chemical vapour deposition cycles, oxidation and wet etching steps; b) Si stripes on insulator waveguides, fabricated by electron-beam lithography and reactive ion-etching (RIE) techniques; c) macroporous Si samples with triangular lattices of holes, prepared by electrochemical etch of a prepatterned substrate. The optical response was measured in the 0.15-3 eV range by transmittance and reflectance with TE and TM polarized light at different angles of incidence $\theta \leq 75^\circ$, and by a white-light Mach-Zehnder interferometer coupled to a Fourier-transform spectrometer. The spectra give clear evidence of the photonic band-gaps and of the quasi-guided modes of the photonic structures, and allow to obtain the photonic band dispersion. The experimental results agree well with the reflectance spectra simulated by the scattering matrix method, and with the photonic bands calculated with an expansion on the basis of plane-waves. A line-shape analysis of the structures in reflectance show that they can be associated to one-dimensional critical points; moreover, a symmetry analysis yields the selection rules for excitation of photonic modes, which can be treated like elementary excitations of the crystal.

1. – Introduction

This paper has been written in memory of Giovanna Panzarini, who actively participated in research on optical properties of radiation-matter interaction at the Department of Physics "A. Volta" for several years.

After the pioneering works about photonic crystals by Yablonovitch [1] and John [2] in 1987, the research in this field has undergone a rapid evolution in the last few years [3, 4, 5] due to the interest both for basic physical phenomena and for applications to optoelectronic and photonic devices (photonic integrated circuits, elements for WDM, low-threshold lasers).

Various materials and techniques have been employed in order to obtain one-, bi-, and tri-dimensional photonic crystals (1D-, 2D-, and 3D-PCs). Although from the theoretical point of view the photonic bands and the optical properties of several 2D and 3D systems are well known from calculations based on plane wave expansion [3, 5], the actual difficulties and the technological challenge consist in fabricating sub-micrometric structures with a photonic gap in the near infrared (NIR) or visible (Vis) energy range. At the moment it is not clear which material is better suited for PC nanotechnologies, however there is no doubt that among high refractive-index materials silicon represents one of the most promising: indeed, Si technology is extremely controlled and is compatible with CMOS integrated applications for electronics.

In this paper we present a synthesis of our work, both experimental and theoretical, performed in the last two years on 1D and 2D silicon-based PCs: previous results or more technical details are reported elsewhere [6, 7, 8, 9].

Three types of PCs have been studied: a) 1D-PCs made of $(\text{Si}/\text{SiO}_2)_m$ multilayers ($m \leq 8$), with layer thicknesses designed to realize $\lambda/4$ distributed Bragg reflectors (DBRs), grown by low-pressure chemical vapour deposition (LPCVD) and oxidation; b) 1D-lattice of Si stripes on insulator (SOI) waveguides, fabricated by electron-beam lithography (EBL) and reactive ion-etching (RIE) techniques; c) 2D macroporous Si samples with triangular lattices of holes, prepared by electrochemical etch of a prepatterned substrate.

The optical properties of these PCs have been measured in the NIR-Vis spectral range by means of the following techniques. i) Transmittance (T) and reflectance (R) with polarized light in order to determine both the energy width of the photonic gaps and the light attenuation in the gaps. ii) Angle resolved R which, as first shown by Astratov *et al.* [10], allows to obtain the dispersion of the photonic bands in 2D-PCs in a waveguide configuration above the light-line. iii) Mach-Zehnder interferometry that measures the optical phase-shift introduced by the sample, and thus directly yields the photonic band dispersion [11].

The experimental measurements are been complemented and addressed by theoretical calculations in the framework of two treatments: R , T , and diffraction simulation via the scattering matrix method [12], and photonic band calculation with plane-wave expansion methods [3, 4].

The choice of the dimensionality and type of the investigated PC structures, as well as of the experimental and theoretical methods, answers to several aims. i) To check the optical quality and uniformity of samples grown and processed by different techniques; ii) to verify the correspondence of the measured properties to the designed ones, in particular to obtain photonic band gaps around 1.3 and $1.55 \mu\text{m}$, which are interesting for fibre communication systems; iii) to apply the angle-resolved R technique to 2D-PCs in a configuration *without* waveguide, and to extend the Mach-Zehnder interferometry, originally introduced by Yablonovitch [11] in the microwave range, to the NIR-Vis range; iv) to analyze the optical response of PCs on the basis of theoretical models, in particular the line-shape of the structures in R spectra corresponding to resonances between incoming light and photonic modes; v) to compare the experimental photonic bands with the calculated ones, and to derive appropriated selection rules, based on symmetry analysis, in order to classify *allowed* and *forbidden* bands.

2. – Experiment

Variable-angle specular reflectance (R) and transmittance (T) were measured in the photon energy range 0.15-3 eV with a Fourier transform spectrometer (Bruker FTIR IFS66/S) at a spectral resolution of 1 meV. The angle of incidence θ was defined with a resolution of $\pm 1^\circ$. A liquid-nitrogen-cooled InSb photodiode was used as a detector and a silver mirror was used as a reference. Measurements at oblique incidence were performed both in transverse electric (TE) and transverse magnetic (TM) polarizations by means of a polypropylene wire-grid polarizer.

Phase sensitive interferometric measurements were performed by means of a home made white-light Mach-Zehnder interferometer coupled to the Fourier-transform spectrometer. The set-up is similar to that introduced in ref. [13] for phase-sensitive ultrashort-pulse interferometry, but it uses a broad-band white-light source (a quartz tungsten-halogen lamp) instead of a fs-laser. Two identical Inconel-coated CaF_2 windows were used as entrance beam-splitter and exit beam-combiner of the Mach-Zehnder interferometer. The system allows a direct measure of the wavelength-dependent phase shift introduced by the sample over a broad spectral range from 0.25 to 2.5 eV.

In the multilayered samples, or in the waveguides before patterning, the composition and the effective layer thicknesses, as well as their lateral uniformity and optical quality of interfaces, were determined by spectroscopic ellipsometry. The ellipsometric functions $\tan \Psi$ and $\cos \Delta$ were measured between 1.4 and 5 eV by a rotating-polarizer ellipsometer (Sopra mod. MOSS ES4G) with a typical standard deviation of less than 0.005, with a mesh of 10 meV and a spectral resolution of 1 meV, at different angles of incidence close to the Brewster angle for optimum sensitivity.

3. – $(\text{Si}/\text{SiO}_2)_m$ 1D-photonic crystals

Si/SiO_2 multilayers were grown in a LPCVD industrial reactor on a 4 in. SiO_2 wafer. The repeatability of layer deposition with LPCVD is one of the most important parameters in order to obtain good DBRs, since the optical transmittance and reflectance critically depend on the layer thickness and periodicity. The processing approach [9, 14] is based on a three-step procedure, which can give reproducible and uniform layers. The first step consisted of a poly-Si deposition on a SiO_2 wafer at 620 °C and with SiH_4 pressure of 280 mTorr. Then, the poly-Si layer was thinned to about 230 nm by a wet oxidation (in H_2 , O_2) at 975 °C. This process resulted in the growth of 140 nm of a- SiO_2 . The SiO_2 layer was then further enlarged by deposition of 500 ± 15 nm SiO_2 (using tetra-ethyl-orthosilicate, TEOS, at 718 °C). These three steps were repeated to achieve $(\text{Si}/\text{SiO}_2)_m$ multilayers with number of periods $m = 2,3,4,6,8$ and with nominal layer thicknesses of 229 nm and 658 nm for poly-Si and SiO_2 layers, respectively. These values were designed in order to realize $\lambda/4$ DBRs, i.e., with the thickness of each layer being inversely proportional to its refractive index.

In Fig. 1(a) typical R , T experimental spectra of $(\text{Si}/\text{SiO}_2)_m$ multilayers, relative to $m = 4$ sample, are shown. Two major features (maxima in R and minima in T) are observed at 1.14 and at 1.81 eV, and are labelled E_{g3} and E_{g5} (the labelling has been chosen in agreement with the theory explained below); two additional minor features E_{g2} at 0.67 and E_{g4} at 1.39 eV are also evident. Similar observations were made for all the samples. The labelled features correspond to the forbidden gaps (the so-called stop-bands) of the 1D photonic structure. Since the multilayers have been grown in the $\lambda/4$ condition, forbidden gaps of odd order (odd index) are wider than even order (even

index) ones as predicted from the theory. The width of E_{g3} and E_{g5} gaps is 18% and 9% of the mid-gap frequency, respectively.

We can also note numerous side bands typical of multilayer interferences. Three major effects with increasing m can be noted in Fig. 2, where T spectra of all samples are reported. The first one is the modification of the shape and amplitude of structures: they become deeper in T spectra (and approach unity in R spectra) indicating an improved rejection ratio both in the even and odd band gaps; moreover the line-shape becomes step-like in the major optical band gaps (E_{g3} and E_{g5}). The second effect is the appearance of extra interference fringes in T (and R) spectra due to the higher number of periods. The third effect is the absorption from poly-Si for energies greater than 1.5 eV, which increases with m due to increasing total poly-Si thickness; the decreasing T intensity reduces practically to zero for all samples beyond 3 eV.

The optical response of the samples was calculated in a full multilayer model (MLM), which implies optically flat and plan-parallel interfaces, using the transfer-matrix method developed by Abèles [9, 15]. The 2×2 complex matrix $\tilde{\mathbf{S}}$ describing light propagation in a multilayer depends in explicit way on the complex refractive index \tilde{n}_j and thickness d_j of each j -layer. \tilde{n}_j of both SiO_2 and poly-Si layers was obtained by SE measurements on single-layer reference samples, grown in the same conditions as the multilayers. The resulting values of \tilde{n}_j for SiO_2 agree very well with those reported in literature [16]. The poly-Si was assumed, in the framework of the Bruggeman effective medium approximation (EMA) [17], as a microscopically heterogeneous material consisting of a random mixture of three separate phases: crystalline silicon, amorphous silicon and voids [9, 18].

R , T and SE spectra were simultaneously fitted to the MLM keeping the poly-Si and SiO_2 layer thicknesses as free parameters. The average values of 220 ± 7 nm for Si and 615 ± 20 nm for SiO_2 , systematically 5% lower than the nominal fabrication thicknesses, were obtained. The comparison between best-fitted curves, obtained from the MLM and the EMA, and experimentally measured spectra have shown a very good agreement [9]; this demonstrates that the layers are homogeneous with sharp interfaces.

The results were compared with theoretical calculation of the 1D photonic band dispersion along the growth axis of the multilayer. Maxwell equations together with the use of Bloch theorem for a 1D periodic structure lead to the following secular equation describing the $\omega(k)$ dispersion [19]

$$(1) \quad \cos kd = \cos k_1 L_1 \cos k_2 L_2 - \frac{1}{n_2} \left(\frac{n_2}{n_1} + \frac{n_1}{n_2} \right) \sin k_1 L_1 \sin k_2 L_2$$

where k is the Bloch vector along the multilayer axis, $d = L_1 + L_2$ is the period and L_j , n_j , $k_j = n_j \omega / c$ ($j = 1, 2$) are thickness, refractive index and wavevector in the layer j , respectively. The $\omega(k)$ dispersion derived from above equation represents the 1D photonic band dispersion for an infinite multilayer. The frequency dependence of n in both SiO_2 and poly-Si can be taken into account by simply letting $n_j \rightarrow n_j(\omega)$. Resulting photonic bands are shown in Fig. 1(b) together with R and T experimental spectra of 4-period multilayer. We note that the calculated photonic gap positions match very well the T minima and R maxima. According to the choice of designing $\lambda/4$ Bragg reflectors, the odd gaps (E_{g1} , E_{g3}), that lie at Brillouin zone edge, are larger while even photonic gaps (E_{g2} , E_{g4}) at the centre of BZ are smaller. The theory shows that, in the case of n independent of frequency, these odd gaps should disappear. In the 0.12-0.25 eV energy range, SiO_2 is highly absorbing due to the transverse optical phonon resonance

as it is evident in experimental spectra where T reduces rapidly to zero; this effect has not taken into account in the calculation of the photonic bands.

The photonic band dispersion of the multilayer structures have been directly measured by means of phase-sensitive interferometry. For the purpose, a fixed white-light Mach-Zehnder interferometer has been coupled to a Fourier transform spectrometer in order to retrieve spectral phase information. The optical phase-shift $\phi(\omega)$ introduced by the sample is determined by the Fourier transform of the cross-correlation interferogram between the sample-arm and the reference-arm of the Mach-Zehnder interferometer [13]. Since $\phi(\omega) = kL$ (where k is the wavevector in the sample and $L = md$ is the total sample thickness), the photon dispersion $\omega(k)$ can be obtained directly from the phase-shift measurement over the entire spectrometer energy interval.

Figure 3 displays the experimental photonic band dispersion in the extended Brillouin zone (up to the 5th zone) for the multilayer sample with $m = 8$. Besides the second and third energy gaps E_{g2} and E_{g3} which are clearly evidenced by undefined phase values, a large dispersion effect is observed for k values near to the band edges where the group velocity $d\omega(k)/dk$ drops down to $c/100$. Notice also the small oscillations in the phase and particularly the slight upturn in correspondence with the E_{g4} zone-centre gap at 1.46 eV. We stress that this result represents a *direct* measurement of the band dispersion of a PC in the NIR-Vis spectral region by the Mach-Zehnder interferometry, that has been previously used only in the microwave region [11].

While the calculated photonic bands are a property of an infinite multilayer, the T and R spectra are obviously taken on samples of finite and different number of periods. This has two consequences. First, the T and R spectra on a sample with m periods display $m - 1$ interference oscillations in the frequency window between two gaps: this corresponds to the 1D photonic bands whose wavevector is discretized according to the total multilayer thickness. Thus each maximum in T should be viewed as due to the excitation of a discretized photonic mode. This explains why the sample with $m = 4$ periods has three transmission maxima between two adjacent gaps (Fig. 1).

Second, the transmittance at the centre of each gap decreases exponentially with m , according to the well-known formula $T \propto (n_L/n_H)^{2m}$ where n_L (n_H) represents the low (high) refractive index. Due to the large refractive index contrast between Si and SiO_2 , low transmittance is obtained already with a small number of periods for the odd gaps E_{g1} , E_{g3} , E_{g5} . In Fig. 4 the minima T values in E_{g3} at 1.14 eV and E_{g5} at 1.81 eV are reported and compared with theoretical values calculated using the transfer matrix method. As expected, increasing number of periods the efficiency of DBR increases. We note that experimental and theoretical T values are in good agreement.

4. – SOI waveguides 1D-photonic crystals

The 1D stripes investigated were obtained by standard electron beam lithography and reactive ion etching techniques on Smart Cut[®] SOI wafers by SOITEC. The thicknesses of silicon and insulator layers were 0.26 μm and 1 μm , respectively. At first, the electron beam patterning was performed by a JEOL 5D2U vector Scan generator operating at 50 keV energy on a single layer of polymethylmetacrylate (PMMA) resist (950 K molecular weight and 150 nm thickness). After development of the PMMA, a thin Nickel layer was evaporated onto the silicon surface and lifted off by dissolution of the PMMA. The reactive ion etching of the Si layer was then performed in a Nextral NE110 system. The etching process used a SF_6/CHF_3 gas mixture at a pressure of 10 mT and a RF power of

15 W. The etching rate was typically 50 nm/min and RIE parameters were optimized for steeper sidewalls. Finally, the remaining Ni mask was removed in a nitric acid solution.

The sample named L4 analyzed in this work is a 1D lattice of stripes, with lattice constant $a=0.65$ μm and 0.18 air fraction. Scanning electron microscope (SEM) image of the sample (Fig. 5) shows the excellent quality of the structure. Spectroscopic ellipsometry measurements were used in a complementary way to characterize the quality and the thickness of the waveguides before patterning.

Variable angle specular reflectance was measured in the spectral range 0.25 - 2 eV. The plane of incidence was (\mathbf{q}, z) , with \mathbf{q} the incoming wavevector and z the perpendicular to the sample surface, and the angle of incidence θ was varied in the 5° - 75° range with a step of 2.5° . Measurements were done for light incident along the $\Gamma - X$ orientation of the 1D crystal (i.e., perpendicular to the stripes) both in transverse electric (TE) and transverse magnetic (TM) polarizations.

Our measurements are based on the surface coupling technique proposed by Astratov et al. [10] on III-V photonic crystals. The method relies on the observation of sharp resonances in R spectra of collimated light incident on the surface of the photonic crystal, when the frequency ω and the parallel wavevector \mathbf{q}_{\parallel} of the incoming beam (which is conserved at the surface and has modulus $\mathbf{q}_{\parallel} = \omega/c \sin \theta$), match ω and \mathbf{k}_{\parallel} of a photonic mode propagating in the plane. Changing θ the matching conditions occur at different ω and \mathbf{k}_{\parallel} : therefore the dispersion of the photonic bands in a given direction can be extracted from the energy positions of the resonances versus \mathbf{k}_{\parallel} that spans the first Brillouin zone.

The experimental results were compared with two complementary theoretical treatments. The photonic bands of the waveguide-embedded photonic crystal were calculated by a newly developed method [7, 8], which consists in expanding the electromagnetic field on the basis of waveguides modes coupled by the off-diagonal terms of the dielectric tensor, where the waveguide is defined to have an average dielectric constant. This method yields not only the photonic modes below the light line, which are truly guided modes and have no diffraction losses, but also the *quasi-guided modes* (or *guided resonances*) above the light line which are probed by the external field in a surface R experiments.

Moreover the reflectance and transmittance (and also the diffraction) of the layered system were calculated by a plane wave expansion in each layer, which yields the complex photonic bands at given \mathbf{k}_{\parallel} and ω , and by propagating the field along the multilayer via a scattering matrix [12]. In the present case we have four layers: air, patterned silicon, unpatterned SiO_2 and Si substrate. The frequency-dependent \tilde{n} of Si and SiO_2 are used in the calculation [16]. We note that this numerical method, which can be applied to any patterned multilayer structure, is an exact solution of Maxwell equations and it contains all diffraction processes in the structure as well as in air.

Experimental and calculated R spectra of sample L4 for TE polarization are shown in Figs. 6(a) and 6(b), respectively. Analogous spectra have been obtained for TM polarization [7].

As a first remark, the experimental R curves show a regular interference pattern resulting from the SOI multilayer waveguide structure. Such interference fringes are related to the effective refractive index of the waveguide and change their period slightly with increasing energy. Superimposed on this interference background, several sharp resonant structures, due to the coupling of the external radiation to the eigenmodes of the photonic crystals, are observed which display a well defined dispersion in their energy positions with increasing θ , and which point to the existence of quasi-guided modes with low losses.

R curves of Figs. 6(a) and (b) display a good overall agreement between experimental and calculated spectra. Both the interference pattern from the core and cladding layers and the observed resonant structures are well accounted for by the calculations, although the calculated resonances appear to be slightly sharper than the experimental ones. This is probably due to some dispersion of the incidence angle which is defined within a cone of $\pm 1^\circ$, and possibly also to some disorder effect coming from the etching process. The intensity and the lineshape of the spectral structures (both experimental and calculated) change with θ , showing a variety of maxima, minima and dispersive-like lineshapes.

The photonic bands derived from R measurements through the aforementioned analysis are plotted in Fig. 6(c) by the dots while the calculated bands are drawn by the solid lines. Since most structures in R spectra show a dispersive-like shape, we take the inflection point as the energy position for the propagating mode. In this way the uncertainty in determining energy bands is estimated to be ~ 5 meV.

Dotted lines represent the dispersion of photons in Si (with the average n of the patterned region) and SiO₂, while dashed lines are the light lines in vacuum. We notice that guided modes, i.e., modes whose dispersion is confined between the Si core and the SiO₂ dispersion lines, are present both for TE and TM polarizations: they arise from a first-order and a second-order waveguide mode. As results from the band diagrams, the lowest band in the guided mode region has a finite cut-off wavelength imposed by the thickness of the asymmetric waveguide. The guided modes go over smoothly into the radiative region when crossing the light line and should thereafter be viewed as resonances or quasi-guided modes. The first-order waveguide mode folded in the radiative region has gaps at the Brillouin zone center and edge; a second-order waveguide mode is also seen to exist in the radiative region with a cutoff energy of about 0.8 eV for TE polarization (1.1 eV for TM polarization). We note that TE modes are odd according to mirror symmetry with respect to the plane of incidence (\mathbf{q}, z).

All the calculated TE and TM bands up to 1.6 eV are recognized in the experimental spectra. In particular, for TE bands the agreement for the dispersion and the energy values is very good, while for TM bands small discrepancies occur which increase with increasing energies. The band diagrams show that a zone-center gap for TE polarization opens around 0.75 eV (1.65 μm), while for TM polarization opens around 0.9 eV (1.38 μm). This can be clearly observed from R spectra: for TE polarization no resonant structure beside interference oscillations is present in the energy interval 0.7 - 0.8 eV for any angle of incidence. This indicates that no photonic mode is allowed in this energy range and therefore propagation through the waveguide is forbidden. A photonic band gap in the radiative region is therefore determined in a more direct way as compared to transmission measurements, where in-plane and out-of plane diffraction as well as symmetry mismatch between incoming and propagating mode may yield low transmission which is not associated to a band gap. The lowest gap at the zone boundary, around 0.45 eV, is formed in the guided mode region: this portion of the $\mathbf{k} - \omega$ space cannot be accessed by surface reflectance, therefore here one has to rely on the calculations.

5. – Macroporous Si 2D-photonic crystals

Macroporous Si samples were prepared by the already well described method of electrochemical etch of a prepatterned substrate [6, 20]. Briefly, triangular and square patterns were defined by photolithography and the initial etch pits were transferred to the substrate by a hot KOH treatment. The successive electrochemical etching in a HF solution allowed to make deeper pores while maintaining their cross-section. Then the sample

was polished with diamond powder to eliminate the etch pits. Substrates of various resistivities were used, both n - and p -type; when the substrate was n -type doped, light assistance was used and provided by a tungsten lamp, which was stabilized in current. Bottom and lateral SEM images, together with the bidimensional Brillouin zone, of a typical triangular pattern are shown in Fig. 7.

Here we present results on a n -type sample with 8-12 Ω -cm resistivity, with triangular structure and lattice constant $a = 2 \mu\text{m}$. The holes have a nearly circular shape with radius $r = 0.24 a$ (air fraction = 0.21).

Unlike waveguide-based photonic crystals, macroporous silicon can be considered as homogeneous along the pore axis (taken as z), since pores of 50 - 100 μm depth can be achieved. The refractive index is modulated only in the xy plane, however the 2D photonic bands retain an out-of-plane dispersion.

Variable-angle specular R measurements, with the plane of incidence (\mathbf{q}, z), were performed along the $\Gamma - K$ and $\Gamma - M$ directions both in transverse electric (TE) and transverse magnetic (TM) polarization. We also calculate R at different angles of incidence by the aforementioned scattering matrix method [12]; in the present case we only have two semi-infinite layers, namely air and patterned silicon. Moreover we calculate the photonic bands of the 2D structure for in-plane propagation using standard plane-wave expansion [3, 21].

In Fig. 8 we show a comparison of measured and calculated reflectance along $\Gamma - K$ for TE and TM polarizations. The R curves of the macroporous Si sample display prominent features with a well-defined dispersion as a function of incidence angle θ . There is a good overall agreement between experimental and calculated spectra for the number of the structures and their angular dispersion, although the experimental lineshape is in some cases more complex than the theoretical one. The spectral strength of the structures depends markedly on the angle θ . Most features become vanishingly weak at $\theta = 5^\circ$, where only one strong structure at 0.29 eV is observed.

The results of Fig. 8 (and the analogous ones along $\Gamma - M$, not shown) are interpreted, like the case of 1D-photonic crystals, as arising from the coupling of the external radiation to the modes of the photonic crystal. However, in the present case, there is no waveguide and a structure in R marks the onset of a photonic mode, which is excited and remains propagating also for higher frequencies (this different behavior is clearly evidenced by comparing the calculated R spectra of Fig. 8 with those of Fig. 6).

It can be seen in Fig. 8 (b,d) that the calculated R spectrum has a discontinuous derivative in correspondence to each structure, like for interband optical transitions at critical-points in semiconductors or insulators. Each critical point in R at energy E_0 is related to a singularity in the diffracted intensity $D(\omega)$, which may be calculated by interpreting the excitation of a photonic mode as an "absorption" process (the intensity of the diffracted beam is removed from specular reflectance and transmittance). Thus $D(\omega) \propto (\hbar\omega - E_0)^{-1/2}$ is obtained, like for a one-dimensional (1D) density of states [6]. The inset of Fig. 8 shows the calculated diffracted intensity of the allowed mode at near-normal incidence, which indeed has the form of an inverse square root close to the threshold $E_0 = 0.29$ eV. A similar behavior is found for all diffracted rays. Thus we conclude that each spectral feature in R corresponds to a 1D critical point.

In order to compare the experimentally determined photonic bands with the theoretical ones we now discuss the selection rules for specular reflectance. The general selection rule can be stated as follows: *a photonic band can appear in reflectance only if it has the same symmetry of the incident electromagnetic field.* The surface of the crystal breaks

mirror symmetry with respect to the xy plane: thus the reflection σ_{xy} is not a symmetry operation anymore. The photonic modes should then be classified according to the subgroup C_{6v} of the point group at Γ and the corresponding subgroups at other k -points. Along the $\Gamma - M$ and $\Gamma - K$ directions the small point group becomes C_s , i.e. specular reflection with respect to the plane of incidence is the only symmetry operation besides the identity.

Now, a TE wave is odd for specular reflection with respect to the plane of incidence, while a TM wave is even. Thus a TE polarized wave interacts with photonic bands which are odd for specular reflection in the vertical mirror plane, while a TM polarized wave interacts only with even bands. Odd photonic bands correspond to Σ_3 and Σ_2 representations of C_{2v} for $\Gamma - M$ (T_3 and T_2 for $\Gamma - K$), while even bands correspond to Σ_1 and Σ_4 for $\Gamma - M$ (T_1 and T_4 for $\Gamma - K$).

In Fig. 9 the photonic bands extracted from R measurements are compared with the calculated ones of the same parity with respect to specular reflection in the plane of incidence. We notice that the experimental points agree very well with the calculated photonic bands of the proper parity. It can be seen that some non-degenerate bands “stop” at the Γ point for a given polarization and “restart” in the other polarization: this peculiar behavior is due to the fact that the mirror plane changes when turning from the $\Gamma - M$ to the $\Gamma - K$ direction. Anticrossings are seen to occur between bands of the same symmetry, e.g., between two Σ_2 states and between two T_2 states around 0.3-0.36 eV.

Not all bands which are allowed by symmetry appear in R curves. This is not in contrast with the selection rule: an allowed band may have a nonzero, yet very weak spectral strength. Indeed, theoretical simulations with a very fine mesh indicate that weaker structures are present, which in the experiments fall below the signal-to-noise ratio.

6. – Conclusions

The experimental results and their overall good agreement with theoretical predictions demonstrate that $(\text{Si}/\text{SiO}_2)_m$ structures have good optical quality and can be designed and used as 1D photonic crystals with high refractive index contrast and good rejection rate even for small m values. This opens new possibilities in terms of patterned (Si/SiO_2) multilayers in order to realize 3D-photonic crystals with a conventional growth technique like LPCVD deposited on Si or SiO_2 substrates. Moreover the use of the Mach-Zehnder interferometry on these structures has demonstrated the real possibility of obtaining directly the band structure of photonic crystals in the near-infrared to visible spectral range.

We have shown that fabrication of photonic crystals on patterned SOI waveguides leads to high-quality structures with well-defined optical properties, as indicated by surface reflectance which displays a number of resonant structures corresponding to the photonic modes. The measured R spectra are well reproduced by those calculated with the scattering matrix method; the photonic bands determined from the spectral positions of resonant structures agree very well with the results of an expansion into waveguide modes of the SOI structure. The present structures are promising in order to obtain a photonic band gap around 1.3 and 1.55 μm wavelengths. Samples with 2D graphite lattice of pillars and triangular lattice of holes are also being fabricated and will be studied in the near future.

Lastly, the experiment on macroporous Si 2D-photonic crystals have shown that photonic bands can be measured by variable-angle reflectance even if no waveguide is present. This opens new possibilities to measure the photonic dispersion even in three-dimensional (3D) photonic crystals. The process for the excitation of a photonic mode has been shown to be similar to the absorption threshold in insulating solids and results in a spectral line-shape analogous to that of critical-point features in semiconductors. The selection rules derived from symmetry have a form similar to those for direct excitation of phonons or excitons, i.e. the photonic modes behave like other elementary excitations in solids. This suggests new interesting research possibilities where spectroscopic studies of material excitations radiatively coupled to photonic modes can be envisaged.

7. – Acknowledgements

This work was supported in part by MURST through PRRIN 2000 project "One- and two-dimensional photonic crystals: growth, theory and optical properties".

REFERENCES

- [1] Yablonovitch E., *Phys. Rev. Lett.*, **58** (1987) 2059.
- [2] John S., *Phys. Rev. Lett.*, **58** (1987) 2486.
- [3] Joannopoulos J.D., Meade R.D., Winn J.N., *Photonic Crystals* (Princeton University Press), 1995.
- [4] Sakoda K., *Optical Properties of Photonic Crystals*, (Springer, Berlin), 2001.
- [5] *Photonic Crystals and Light Localization in the 21st Century* edited by C.M. Soukoulis (Kluwer, Dordrecht), 2001.
- [6] Galli M., Agio M., Andreani L.C., Belotti M., Guizzetti G., Marabelli F., Patrini M., Bettotti P., Dal Negro L., Gaburro Z., Pavese L., Lui A., and Bellutti P., *Phys. Rev. B*, **65** (2002) 11311.
- [7] Patrini M., Galli M., Marabelli F., Agio M., Andreani L.C., Peyrade D. and Chen Y., *IEEE J. Quantum Electron.*, **38** (2002), in press.
- [8] Andreani L.C. and Agio M., *IEEE J. Quantum Electron.*, **38** (2002), in press.
- [9] Patrini M., Galli M., Belotti M., Andreani L.C., Guizzetti G., Pucker G., Lui A., Bellutti P. and Pavese L., *J. Appl. Phys.*, (2002), in press.
- [10] Astratov V.N., Whittaker D.M., Culshaw L.S., Stevenson R.M., Skolnick M.S., Krauss T.F., De La Rue R.M., *Phys. Rev. B*, **60** (1999) R16255.
- [11] Yablonovitch E. and Gmitter T.J., *Phys. Rev. Lett.*, **63** (1989) 1950.
- [12] Whittaker D.M. and Culshaw L.S., *Phys. Rev. B*, **60** (1999) 2610.
- [13] Kop R.H.J. and Sprik R., *Rev. Sci. Instrum.*, **66** (1995) 5459; Imhof A., Vos W.L., Sprik R., and Lagendijk A., *Phys. Rev. Lett.*, **83** (1999) 2942.
- [14] Pucker G., Bellutti P., Spinella C., Gatterer K., Cazzanelli M., and Pavese L., *J. Appl. Phys.*, **88** (2000), 6044.
- [15] Abelès F., *J. de Phys.*, **11** (1950) 310.
- [16] *Handbook of optical constants of solids* edited by E.D. Palik (Academic Press, Orlando), 1985.
- [17] Garnett J.C.M., *Philos. Trans. R. Soc. London*, **203** (1904) 385; **A 203** (1906) 237.
- [18] Petrik P., Lohner T., Fried M., Birò L.P., Khàn N.Q., Gyulai J., Ryssel H., *J. Appl. Phys.*, **87** (2000), 4.
- [19] Yariv A. and Yeh P., *Optical waves in crystals*, (Wiley, New York) 1984.
- [20] Gruning U., Lehmann V., Ottow S., Busch K., *Appl. Phys. Lett.*, **68** (1996) 747; Birner A., Wehrspohn R.B., Gosele U., Busch K., *Adv. Mater.*, **13** (2001) 377.
- [21] Ho K.M., Chan C.T., Soukoulis C.M., *Phys. Rev. Lett.*, **65** (1990) 3152.

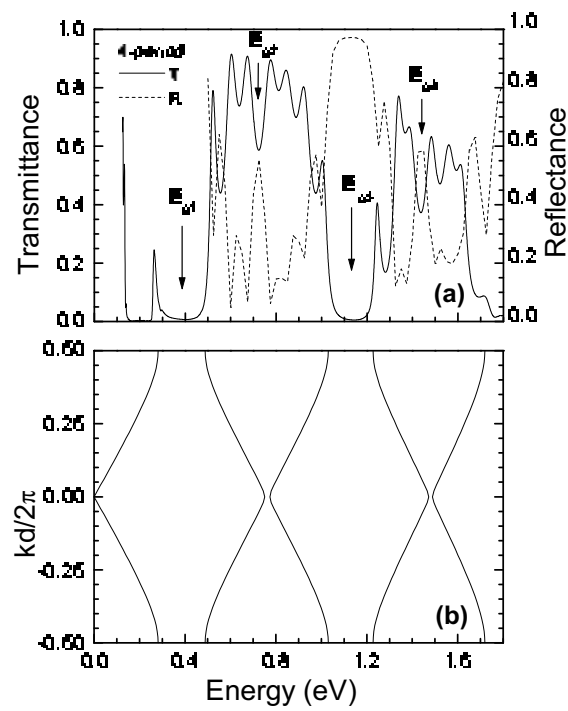


Fig. 1. – (a) Optical response in reflectance (dotted) and transmittance (solid) of the 4-period $(\text{Si}/\text{SiO}_2)_4$ sample compared to photonic band dispersion (b) calculated for an infinite 1D Si/SiO_2 photonic crystal in the same spectral range. The energies at the center of the photonic gaps are marked by arrows.

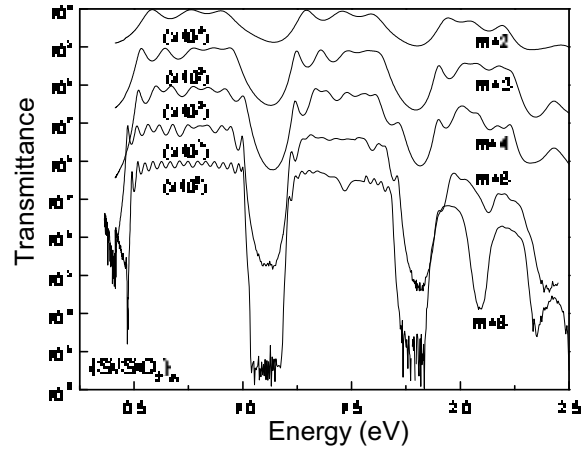


Fig. 2. – Transmittance spectra of 1D- $(Si/SiO_2)_m$ photonic crystals for $m = 2, 3, 4, 6, 8$.

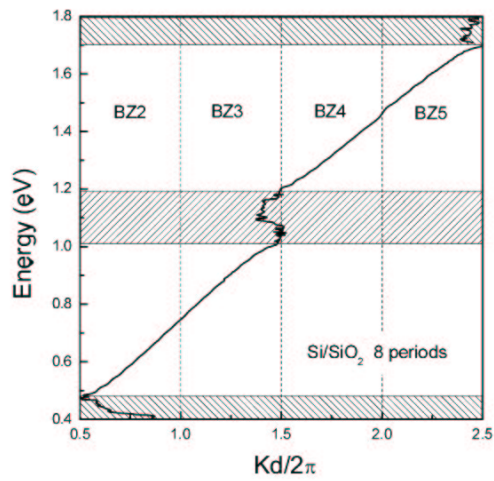


Fig. 3. – Photonic band dispersion of the $(Si/SiO_2)_{m=8}$ sample measured by the Mach-Zehnder interferometry.

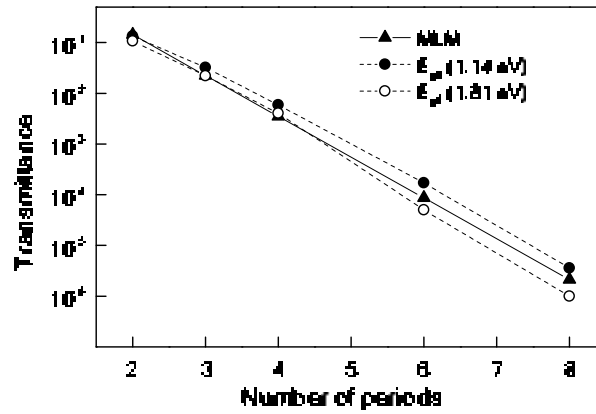


Fig. 4. – Transmittance values at the middle of the photonic gaps E_{g3} and E_{g3} (solid and open circles, respectively) in $(\text{Si}/\text{SiO}_2)_m$ photonic crystals versus the period number m . T values as calculated by the full multilayer model are also reported (up triangles).

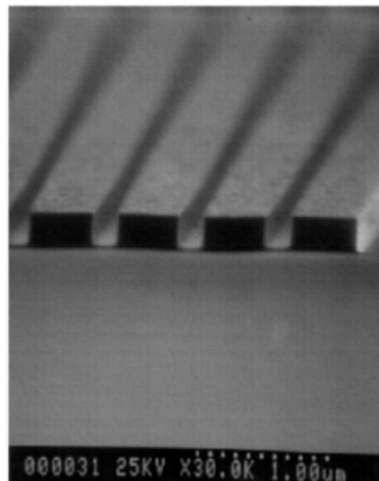


Fig. 5. – SEM micrograph of sample L4 (side view) made of 1D-lattice of Si stripes on Si/SiO_2 , with lattice constant $a=0.65 \mu\text{m}$ and 0.18 air fraction.

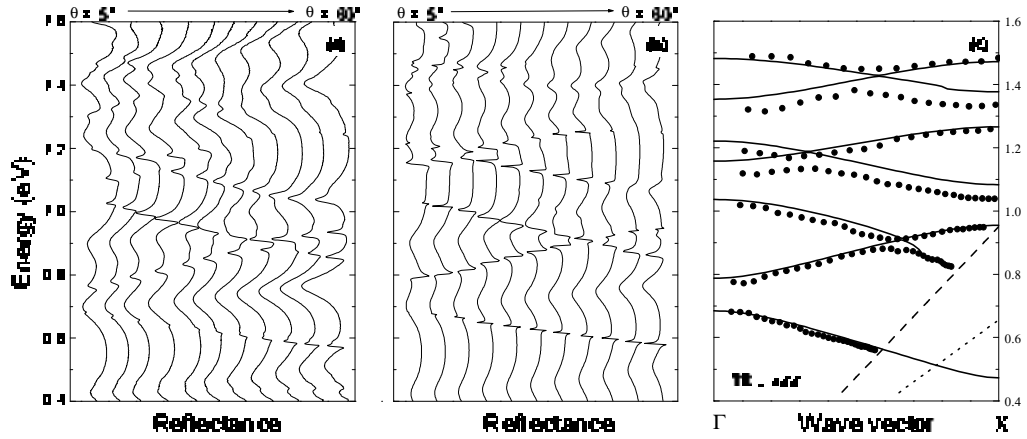


Fig. 6. – TE reflectance spectra from $\theta = 5^\circ$ to 60° in step of 5° for sample L4: (a) experimental and (b) calculated. (c) Photonic bands of sample L4, calculated (solid lines) and determined from the experimental R spectra (dots). Dotted (dashed) lines: dispersion of light in Si, SiO_2 (in air).

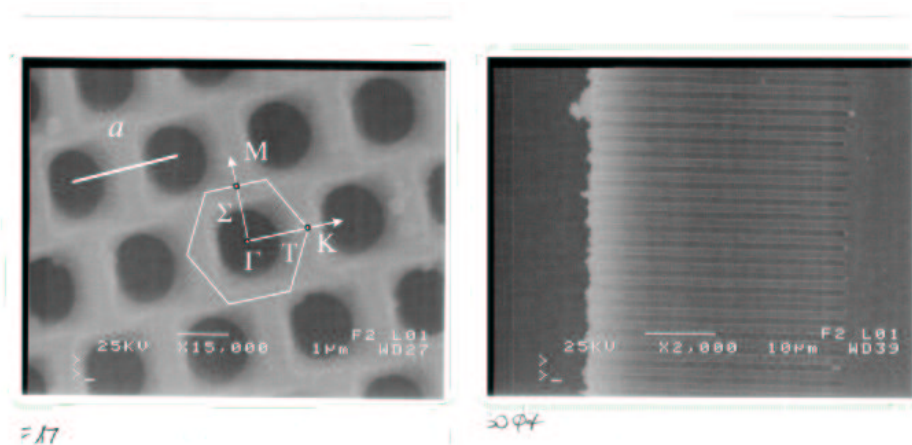


Fig. 7. – Top and lateral SEM images of a patterned macroporous silicon forming a 2D triangular lattice. The bidimensional Brillouin zone is also indicated in the left panel (notice that the size is arbitrary, since it is superimposed on the real-space structure).

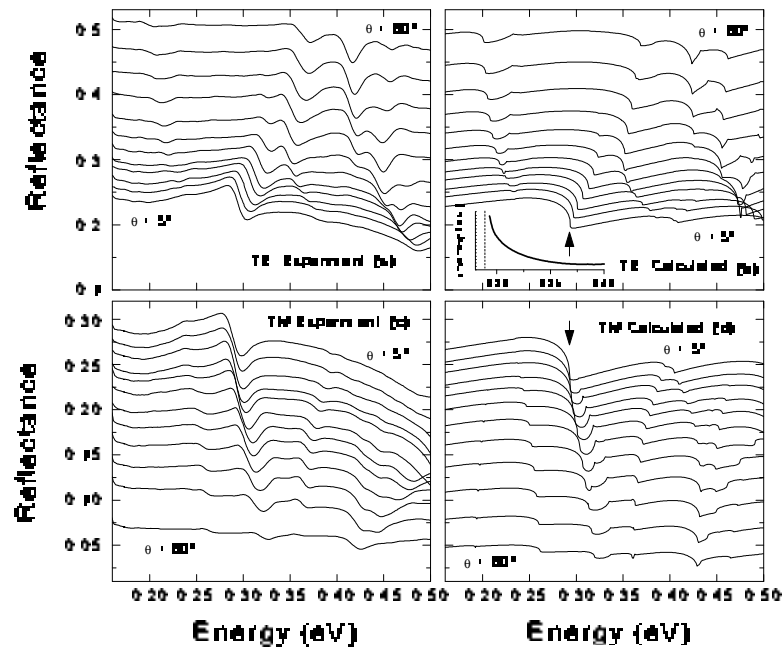


Fig. 8. – (a), (c): Experimental reflectance of 2D macroporous silicon for light incident along the $\Gamma - K$ orientation, for TE and TM polarizations; (b),(d): calculated reflectance. The angle of incidence θ is varied from 5° to 60° with a step of 5° . The curves at 5° , 10° and 15° are slightly offset for clarity. Inset to (b): diffracted intensity corresponding to the allowed mode at $\theta = 5^\circ$ (onset marked by arrows).

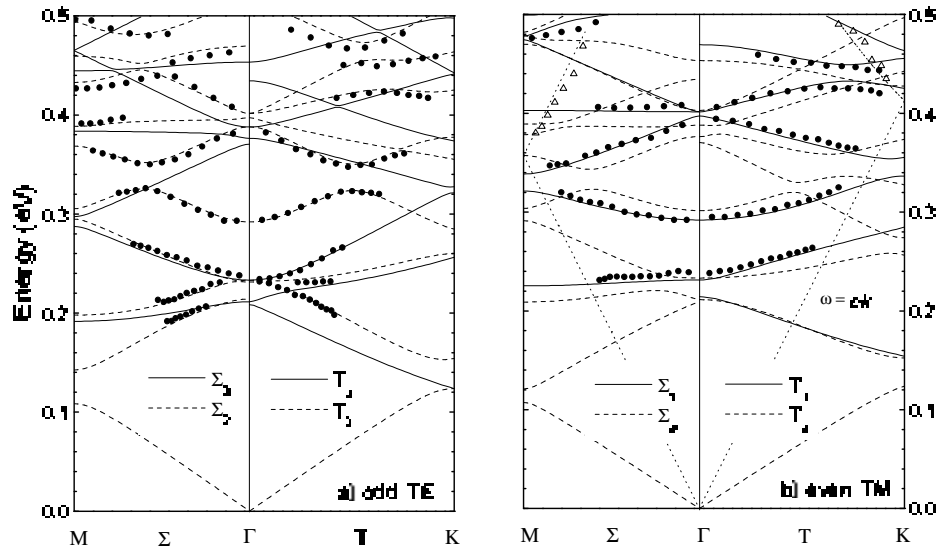


Fig. 9. – Points: measured dispersion of the photonic bands of 2D macroporous silicon, derived from the structures in reflectance curves; solid and dashed lines: calculated photonic bands, separated according to parity with respect to the plane of incidence: (a) TE polarization - odd modes, (b) TM polarization - even modes. The open triangles in (b) represent diffraction in air and must be compared with the folded dispersion of free photons (dotted lines).